ISSN (Print) 1226-1750
ISSN (Online) 2233-6656
Journal of Magnetics 22(3), 353-359 (2017) https://doi.org/10.4283/JMAG.2017.22.3.353

Synthesis and Physicochemical Studies of Perovskite Manganite $La_{0.8}Ca_{0.2}Nn_{1-x}Co_xO_3$ ($0 \leq x \leq 0.3$)

D. Turki[1,4], Zafar Khan Ghouri[2]*, Saeed Al-Meer[2]*, Khaled Elsaid[3], M. I. Ahmad[2], Ahmed Easa[2], M. Ellouze[4], and E. K. Hlil[5]

[1]*Department of Chemistry & Earth Sciences, College of Arts & Science, Qatar University, P.O. Box: 2713, Doha, Qatar*
[2]*Central Laboratories Unit, Qatar University, P.O. Box: 2713, Doha, Qatar*
[3]*Chemical Engineering Program, Texas A&M University at Qatar, P.O. 23874, Doha, Qatar*
[4]*University of Sfax, Faculty of Sciences of Sfax, B.P. 1171, Sfax 3000, Tunisia*
[5]*InstitutNéel, BP 166, F-38042 Grenoble Cedex 9, France*

(Received 17 April 2017, Received in final form 28 July 2017, Accepted 4 August 2017)

The physicochemical properties of $La_{0.8}Ca_{0.2}Mn_{1-x}Co_xO_3$ nanopowders as a function of Co content (x) have been investigated. $La_{0.8}Ca_{0.2}Mn_{1-x}Co_xO_3$ nanopowders were synthesized by sol-gel method and morphologically and structurally well characterized by Scanning electron microscopic (SEM), Infrared spectroscopic (IR) and Raman spectroscopic techniques. IR spectra shows peak at around 600 cm^{-1} attributed to the stretching mode of MnO_6 octahedral and peak at 700 cm^{-1} assigned to La-Ca-O-Mn bending vibrations. Raman spectra indicate peaks at around 512 and 652 cm^{-1} related to the Jahn-Teller octahedral distortions. The intensity of these peaks increases with increasing Co doping. The UV-visible spectra were measured in the frequency range of 200-800 nm and two energy gaps were found at 1.63 eV and 3.294 eV for x = 0, 0.1 and 0.3.

Keywords : Nanopowders, Perovskite, Scaning electron microscopy (SEM), Raman spectroscopy, IR spectroscopy, UV-visible measurement

1. Introduction

The doped rare-earth manganites are an example of partial structural disorder. This disorder varies strongly with doping level and temperature. Monitoring of the disorder is of significant interest for understanding the interplay of transport, magnetic, and structural properties [1-7]. The perovskite-like manganese materials are distorted from perfect cubic symmetry, so phonons should be observed in all spectra due to either the distortion or the compositional disorder associated with the introduction of non-stoichiometric materials [8]. Generally, in the perovskite manganite structure, the A-site cation is surrounded by 12 oxygen ions whereas the B-site cation is bonded to six oxygen ions in the octahedral interstices of the oxygen sub-lattice. Mismatch between the A-O and B-O equilibrium bond lengths introduces internal stresses. In fact, the perovskite distortions can be divided into two groups: distortions changing Mn-O-Mn bond angles and distortions changing the Mn-O distances governed by the magnitude and the spatial coherence of the Jahn-Teller distortions of the MnO_6 octahedra [9, 10]. Infrared (IR) and Raman spectroscopic studies of the system with simultaneous doping of both A and B site is often a necessary tool and useful supplement for X-ray diffraction to understand the vibration modes of the manganese oxides. Basically, IR spectroscopy is a tool for mineralogical analysis since it is sensitive to amorphous components and to short-range and long range order in materials. In addition, it is sensitive to the local lattice distortions [11, 12]. IR spectroscopy would reveal a more complete and reliable description of materials such as the manganese oxides, where crystalline disorder may be expected. In fact, there have been numerous reports on the variation of the IR spectra in doped $La_{1-x}R_xMnO_3$ systems [13-17] and most of these were carried out with polycrystalline samples. Okimoto *et al.* [18] measured optical spectra of a single crystal $La_{1-x}Sr_xMnO_3$ but its

*Co-corresponding author: Tel: +97450587742,
Fax: +97444034669, e-mail: zafarkhanghouri@hotmail.com
zafarkhan.ghouri@qu.edu.qa
salmeer@qu.edu.qa

phonon spectra were not studied in detail. Kim *et al.* measured IR phonon spectra of a polycrystalline $La_{0.7}Ca_{0.3}MnO_3$ [19]. The bending and stretching modes of the MnO_6 octahedral are identified near the metal-insulating (MI) transition and explained in terms of a polaron model. Moreover, the important role of electron-phonon coupling in the lattice dynamics of the manganese has been proved.

Raman spectroscopy is a powerful tool for the study of structural disorders, vibrational, electronic excitations, phase transitions, lattice transformation and doping levels [20, 21]. The lattice dynamical calculations and assignment of the Raman modes of $LaMnO_3$ were done previously by Iliev *et al.* [22] then by Grando *et al.* [9]. So far, there have been numerous reports on the variations of the Raman spectra of $Ln_{1-y}R_yMn_{1-x}M_xO_3$ (Ln-rare earth, R = Ca, Sr, Ba, M = Co, Fe, Cr, Zn….) [23-27]. According to Iliev *et al.* [22] there are 24 Raman-allowed modes ($7A_g + 5B_{1g} + 7B_{2g} + 5B_{3g}$) for the orthorhombic $La_{1-x}Ca_xMnO_3$ with Pnma space group. The observed modes at 140, 198, 257, 284 and 493 cm^{-1} were assigned as A_g symmetry, modes at 109, 170, 308, 481 and 611 cm^{-1} as B_{2g} and modes at 184 and 320 cm^{-1} as B_{1g} or B_{3g}. Phong *et al.* [28] have measured Raman spectra of $La_{0.8}Sr_xCa_{0.2-x}MnO_3$ at room temperature in the range of 100-700 cm^{-1} and found that all spectra exhibit three broad bands in the interval of 190-250, 420-500 and 550-650 cm^{-1}. For $x = 0$ they have observed bands at 231.97, 311.51, 450.74, 494.39 and 638.16 cm^{-1}. The mode at 231.97 cm^{-1} with A_g symmetry is ascribed to an in-phase rotational vibration of the MnO_6 octahedra about the y axis. The mode at 311.51 cm^{-1} corresponds to an out-of-phase vibration of the MnO_6 octahedra about the x axis. The mode at 450.74 cm^{-1} is a B_g bending mode (pure oxygen out-of-phase bending vibration). The mode at 494.39 cm^{-1} is associated with an out-of-phase stretching vibrations of the octahedral and is associated with the Jahn-Teller distortion of the octahedra. Finally, the 638.16 cm^{-1} mode, called the breathing mode, is due to bending vibrations of the octahedra.

The important reason to analyze the structure of the manganites is to understand the basic mechanism by which the magneto-transport properties can be tuned at doping level. In this work, the effect of Co doping on the physical properties of $La_{0.8}Ca_{0.2}Mn_{1-x}Co_xO_3$ manganite has been investigated by means of various spectroscopic techniques.

2. Experimental

In order to synthesize $La_{0.8}Ca_{0.2}Mn_{1-x}Co_xO_3$ (x = 0, 0.1, 0.2 and 0.3) nanopowders, precursors (La_2O_3, CaO, MnO_2 and Co_3O_4) were dissolved in deionized water under vigorous stirring, and then appropriate amounts of nitric acid (HNO_3), ethylene glycol and citric acid were added and the mixture kept stirring for 60 min at 90 °C in order to get transparent sol-gel solution, after which the resulting sol-gel dried at 180°C to get the desired powder. Then as-prepared powders were milled and calcined at 1000°C for 3 h.

The morphology and elemental distribution was evaluated using scanning electron microscopy (SEM, Zeiss Ultra$^+$) equipped with energy dispersive X-ray analysis (EDAX). Raman spectra of sintered samples was recorded from 50 to 800 cm^{-1} in a micro-Raman spectrometer (LABRAM HR-800), working in a back scattering configuration, equipped with a He^+ ion ($\lambda = 633$ nm) laser while Fourier Transform Infrared (FTIR) spectra of as-prepared samples was obtained from a Bruker, Tensor 37 spectrometer, using KBr pellets.

3. Discussion

The perovskite phase of $La_{0.8}Ca_{0.2}Mn_{1-x}Co_xO_3$ has Pnma symmetry (D_{2h}^{16}), with four formula units per unit cell [13, 30, and 31]. The La/Ca atoms occupy the 4c Wyckoff positions, the Mn/Co atoms occupy the 4b Wyckoff positions and the O atoms occupy the 4c and 8d Wyckoff positions. According to group theory there are 60 phonon modes at Γ decomposed as irreducible representations:

$$\Gamma = 7A_g + 5B_{1g} + 7B_{2g} + 5B_{3g} + 8A_u + 10B_{1u} + 8B_{2u} + 10B_{3u}$$

Except for the A_u modes, all the other u modes are infrared active and all the g modes are Raman active. For single crystal Raman, the A_g modes are visible no matter the crystal orientation, whereas the B modes are sensitive to the crystal orientation with respect to the polarization of the light.

3.1. X-ray data and T_C

Figure 1 displays the effect of Co doping on lattice parameters, volume of the elementary cell and transition temperature T_C. It can be seen, in the case of Co doping ($0 \le x \le 0.2$), the lattice parameters (a & b) and unit cell volume increases while in case of Co doping ($0.2 \le x \le 0.3$) both lattice parameters (a & b) and unit cell volume decrease. On the other hand lattice parameter (c) decreases with increasing Co-doping. Moreover, a steep decrease in transition temperature (T_C) was also observed with 0.01 % Co doping [29].

One can claim that the transition temperature decreases

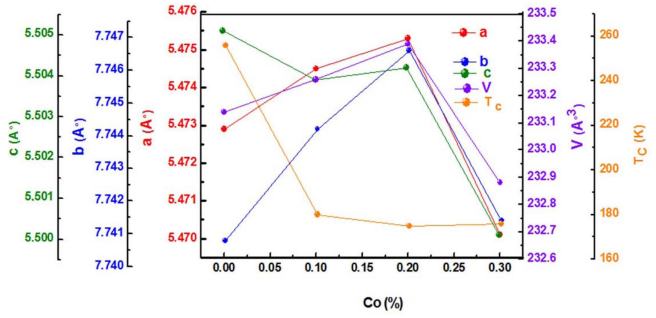

Fig. 1. (Color online) Effect of Co doping on lattice parameters, volume of the elementary cell and transition temperature.

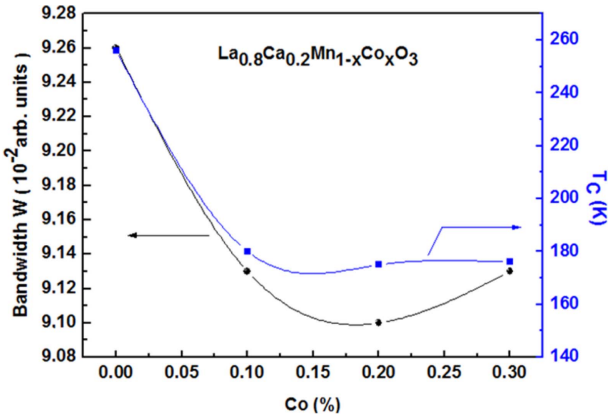

Fig. 2. (Color online) Effect of Co doping on bandwidth (W).

Table 1. The average bond length Mn-O, the average bond angle <Mn-O-Mn>, the unit cell volume, the one-electron bandwidth W, the Curie temperature T_C and the average grain size GS for $La_{0.8}Ca_{0.2}Mn_{1-x}Co_xO_3$ nanopowders.

$La_{0.8}Ca_{0.2}Mn_{1-x}Co_xO_3$	$x = 0$	$x = 0.1$	$x = 0.2$	$x = 0.3$
<Mn-O-Mn> (°)	162.134	161.108	161.562	161.168
Mn-O (Å)	1.966	1.973	1.976	1.973
W/W_0 ($\times 10^{-2}$)	9.26	9.13	9.1	9.13
T_C (K)	256	180	175	176
GS (nm)	294	419	733	558

due to the double exchange (Mn^{3+}–O^{2-}–Mn^{4+}) and super exchange interaction (Mn^{3+}–O^{2-}–Mn^{3+}) [32]. However it can be assumed that the ferromagnetic ordering temperature is disturbed due to the substitution of Co in the $La_{0.8}Ca_{0.2}Mn_{1-x}Co_xO_3$ system [33].

For perovskite compounds with general formula ABX_3, the electronic bandwidth W depends on both the B-X-B bond angles and B-X bond lengths, through the overlap integrals between the 3d orbital of the metal ion B and the

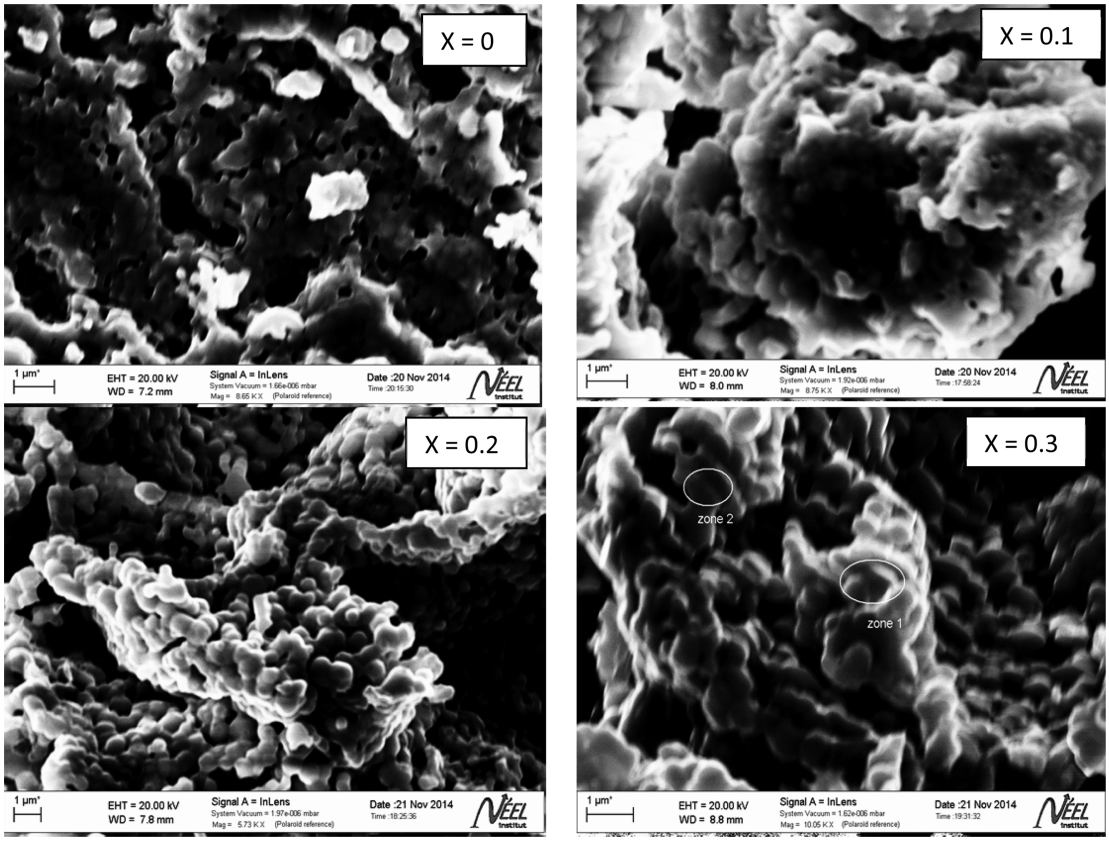

Fig. 3. SEM micrographs of $La_{0.8}Ca_{0.2}Mn_{1-x}Co_xO_3$ ($0 \leq x \leq 0.3$) nanopowders.

2p orbital of the X anion. The following formula has been used to describe this double dependence [34]:

$$\frac{W}{W_0} = \frac{Cos(v)}{\langle d_{B-X} \rangle^{3.5}}$$

Where $v = \frac{\pi - \langle B-X-B \rangle}{2}$ is the "tilt" angle in the plane of the bond, and $d_{B\text{-}X}$ is the B-X bond length. The calculated values are presented in Table 1. The evolution of W as a function of Co doping is remarkably similar to that of T_C (Fig. 2).

3.2. Scanning Electron Microscopy

The SEM images of $La_{0.8}Ca_{0.2}Mn_{1-x}Co_xO_3$ (x = 0, 0.1, 0.2, and 0.3) nanopowders are shown in Fig. 3(a-d). The images clearly show the presence of grains with good connectivity. Mostly grains are spherical in shape with grain sizes ranging from 200 to 300 nm with homogeneous particle size distributions [35]. The average particle/grain sizes (Gs) are summarized in Table 1.

Furthermore, energy dispersive X-ray analysis (EDAX) maps (Fig. 4) obtained from zone 1 & 2 of Fig. 3 confirms that the nanopowders contains La, Ca, Mn, O and Co; no other elemental contamination was detected. Chemical compositions of $La_{0.8}Ca_{0.2}Mn_{1-x}Co_xO_3$ (x = 0, 0.1, 0.2, and 0.3) nanopowders obtained by EDAX are summarized in the inset in Fig. 4.

3.3. Infrared spectra

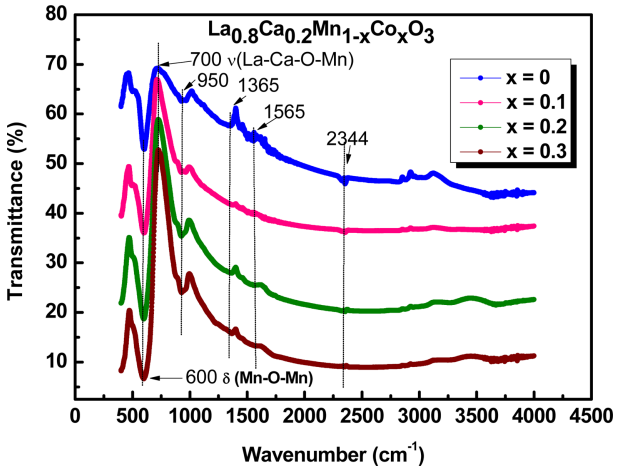

Fig. 5. (Color online) Infrared spectra of $La_{0.8}Ca_{0.2}Mn_{1-x}Co_xO_3$ ($0 \le x \le 0.3$) nanopowders.

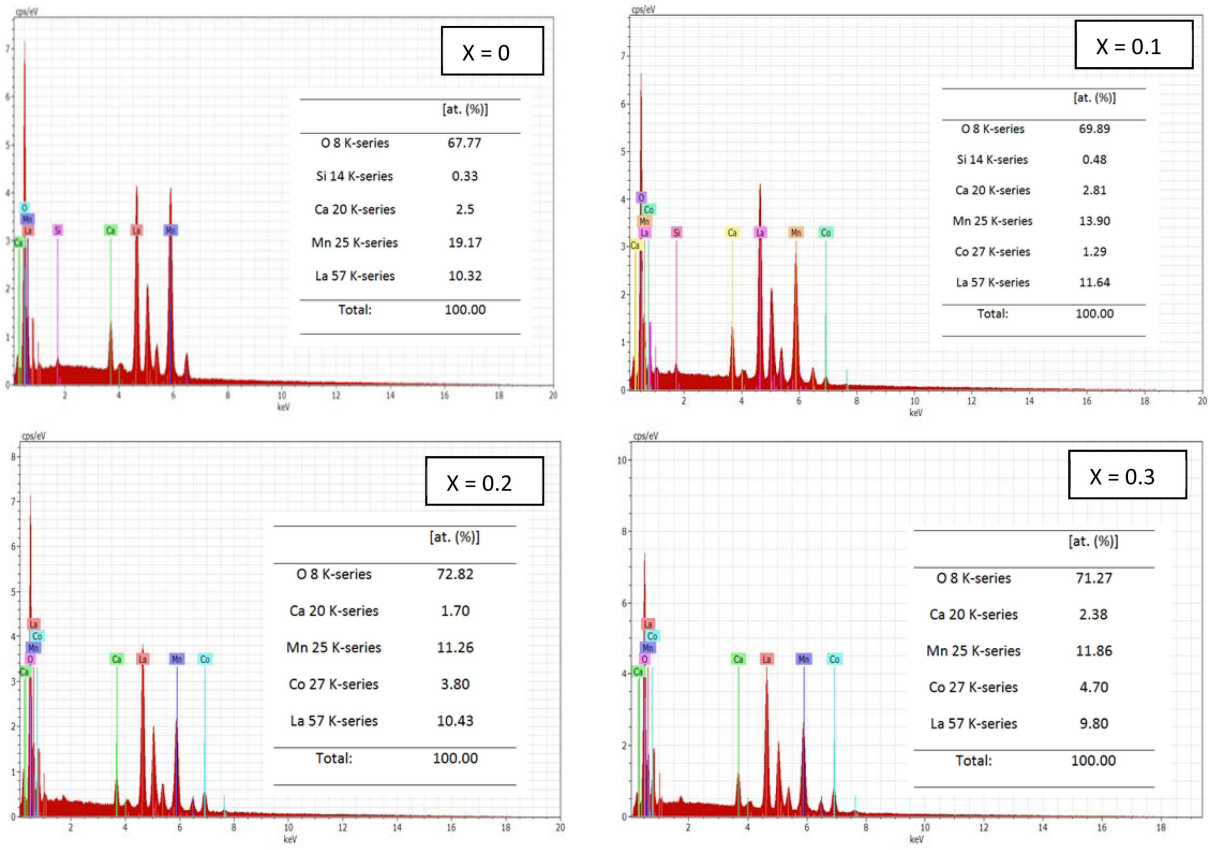

Fig. 4. (Color online) EDAX spectra of $La_{0.8}Ca_{0.2}Mn_{1-x}Co_xO_3$ ($0 \le x \le 0.3$ nanopowders.

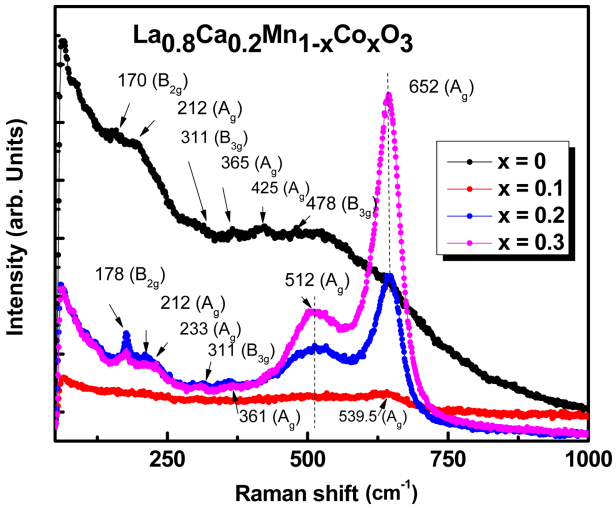

Fig. 6. (Color online) Raman spectra of $La_{0.8}Ca_{0.2}Mn_{1-x}Co_xO_3$ ($0 \leq x \leq 0.3$) nanopowders at room temperature in the spectral range 50-1000 cm^{-1}.

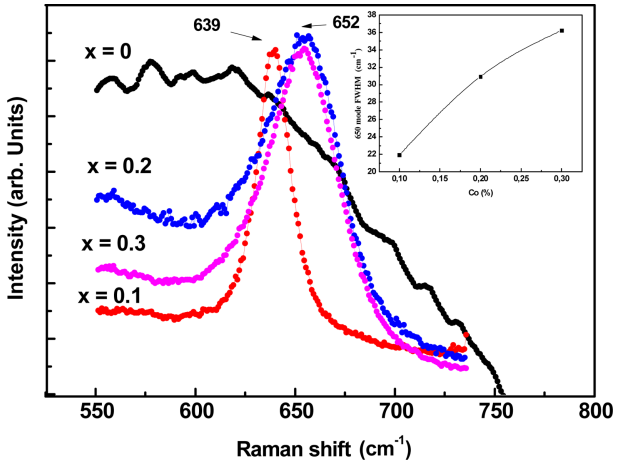

Fig. 7. (Color online) Effect of Co doping on Raman spectra of $La_{0.8}Ca_{0.2}Mn_{1-x}Co_xO_3$ nanopowders near 650 cm^{-1}. The inset shows behavior of the FWHM 650 cm^{-1} mode with respect to Co doping.

The IR absorption spectra of $La_{0.8}Ca_{0.2}Mn_{1-x}Co_xO_3$ (x = 0, 0.1, 0.2, and 0.3) nanopowders was measured at room temperature (Fig. 5). According to group theory, there are 25 IR-active modes ($9B_{1u} + 7B_{2u} + 9B_{3u}$) [36]. However, Smirnova *et al.* [14] found only 11 modes at the lowest

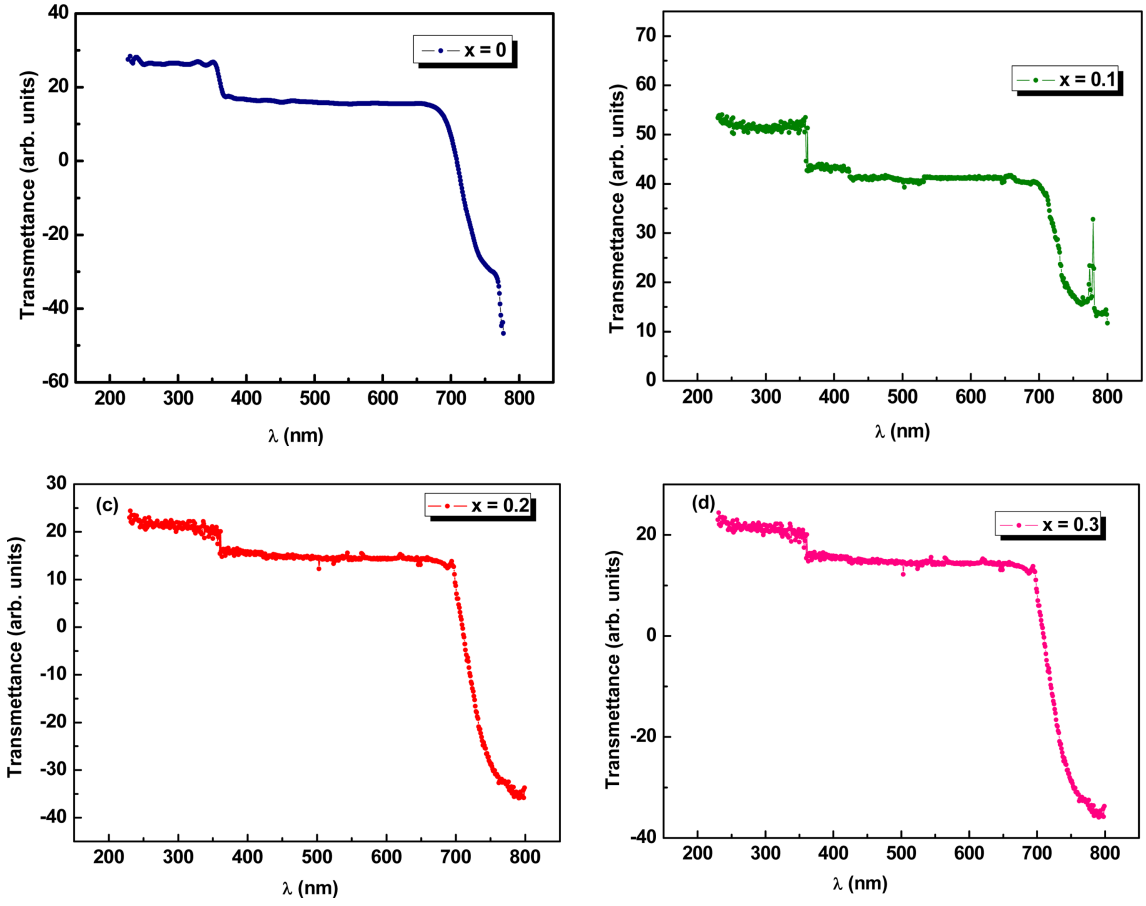

Fig. 8. (Color online) UV-visible transmission spectrum of $La_{0.8}Ca_{0.2}Mn_{1-x}Co_xO_3$ nanopowders.

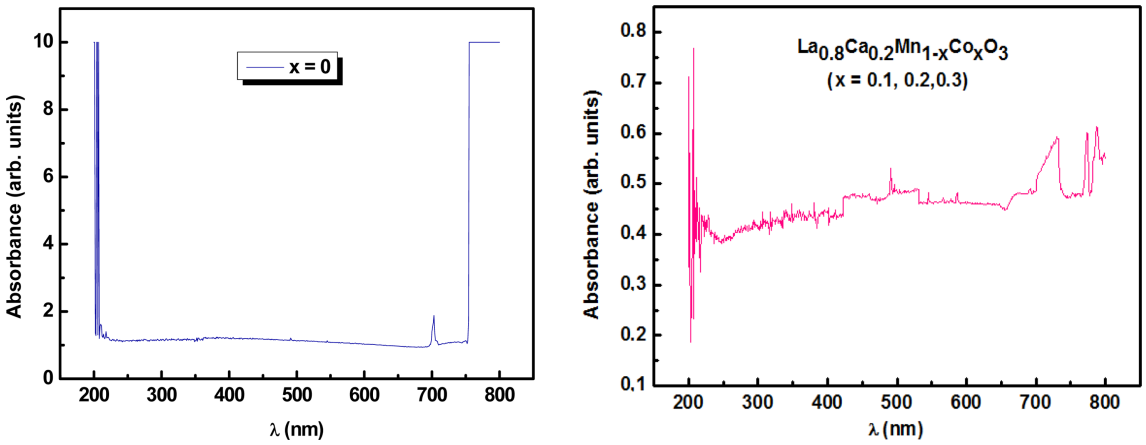

Fig. 9. (Color online) UV-visible absorption spectrum of $La_{0.8}Ca_{0.2}Mn_{1-x}Co_xO_3$ nanopowders.

frequencies (100 cm^{-1} - 250 cm^{-1}). $La_{0.8}Ca_{0.2}Mn_{1-x}Co_xO_3$ nanopowders shows various peaks at around 2344, 1565, 1365 and 950 cm^{-1}. The peaks observed at 950, 1365, 1565 cm^{-1} are attributed to metal-oxygen vibrations while the peak observed at 2344 cm^{-1} is associated with symmetric and asymmetric stretching vibrations of -CH_3 groups [38]. Moreover, the peak at around 600 cm^{-1} corresponds to the stretching mode, which arises due to the vibration modes of the MnO_6 octahedra [37] and the peak observed at 700 cm^{-1} is related to La-Ca-O-Mn bending vibrations [38].

3.4. Raman Scattering

Raman spectra were measured at room temperature (Fig. 6) and discussed based on the previous literature [27, 39, and 40]. For $x = 0$, six characteristic bands are observed at around 170, 212, 311, 365, 425 and 478 cm^{-1}. The bands at 212, 365 and 425 cm^{-1} correspond to the A_g mode; the bands at around 311 and 478 cm^{-1} are associated with B_{3g} mode while the band at 170 cm^{-1} is attributed to B_{2g} modes. For $x = 0.1$, only one characteristic band at 539.5 cm^{-1} corresponding to A_g symmetry was observed.

Moreover, the phonon bands for $x = 0.2$ and $x = 0.3$ are identical and we believe that the band at 178 cm^{-1} is associated with B_{2g}, the bands at 212, 233, 361, 512 and 652 cm^{-1} correspond to A_g and the band at 311 cm^{-1} is related to B_{3g} modes. Indeed, the two bands at 512 and 652 cm^{-1} were related to the Jahn-Teller octahedral distortions.

Figure 7 shows the effect of Co-content on the Raman spectra of $La_{0.8}Ca_{0.2}Mn_{1-x}Co_xO_3$ near 650 cm^{-1}.

It can be perceived that the Raman band is shifted from lower to higher frequency (639 cm^{-1} to 652 cm^{-1}) with increasing Co-doping. This finding is consistent with the behavior of the FWHM of the 650 cm^{-1} mode [41] as shown in the inset image of Fig. 7.

UV-Visible Spectroscopy

To study the optical properties of $La_{0.8}Ca_{0.2}Mn_{1-x}Co_xO_3$ (x = 0, 0.1, 0.2, and 0.3) nanopowders, UV-visible spectroscopy measurement has been done. UV-visible transmittance spectra shows identical results for both $x = 0.2$ and $x = 0.3$ (Fig. 8). Similarly, results obtained from UV-visible absorption spectra are identical for $x = 0.1$, $x = 0.2$ and $x = 0.3$ (Fig. 9). However, spectra obtained from UV-visible absorption spectroscopy for the undoped powders is different than that of doped powders (Fig. 9) which is acceptable due to the difference in magnetic properties [7, 29].

Moreover, $La_{0.8}Ca_{0.2}Mn_{1-x}Co_xO_3$ nanopowders have a strong photo absorption property in the visible light region. The corresponding band gap energies are estimated to be about 1.6 eV and 3.294 eV (Fig. 8), which is comparable with results obtained from the literature [42-45]. Consequently, $La_{0.8}Ca_{0.2}Mn_{1-x}Co_xO_3$ nanopowders may serve as a good photocatalyst for environmental remediation.

4. Conclusion

$La_{0.8}Ca_{0.2}Mn_{1-x}Co_xO_3$ nanopowders were synthesized by sol-gel method and morphological and structural properties as a function of Co content (x) have been investigated by Scanning electron microscopic (SEM), Infrared spectroscopic (IR) and Raman spectroscopic techniques. Due to strong photo absorption property in the visible light region, the introduced $La_{0.8}Ca_{0.2}Mn_{1-x}Co_xO_3$ nanopowders may serve as a promising material for photocatalytic reactions.

References

[1] Philip. B. Allen and V. Perebeinos, Phys. Rev. B **60**, 15 (1999).
[2] D. Lim, V. K. Thorsmølle, R. D. Averitt, Q. X. Jia, K. H. Ahn, M. J. Graf, S. A. Trugman, and A. J. Taylor, Phy. Rev. B 71, 134403 (2005).
[3] G. Bouzerar and O. Cépas Phys. Rev. B **76**, 020401 (R) (2007).
[4] J. C. Debnath, R. Zeng, J. H. Kim, P. Shamba, D. P. Chen, and S. X. Dou, J. Alloys Compd. **510**, 125 (2012).
[5] A. Nasri, S. Zouari, M. Ellouze, J. L. Rehspringer, A. F. Lehlooh, and F. Elhalouani, J. Supercond. Nov. Magn. **5**, 2282 (2013).
[6] S. Zouari, M. Ellouze, E. K. Hlil, F. Elhalouani, and M. Sajieddine, Solid State Comm. **180**, 16 (2014).
[7] D. Turki, G. Remenyi, S. H. Mahmood, E. K. Hlil, M. Ellouze, and F. Halouani, Mat. Res. Bul. **84**, 245 (2016).
[8] A. E. Pantoja, H. J. Trodahl, R. G. Buckley, Y. Tomioka, and Y. Tokura, J. Phys.: Condens. Matter. **13**, 3741 (2001).
[9] E. Granado, A. Garcıa, J. A. Sanjurjo, C. Rettori, and I. Torriani Phys. Rev. B **60**, 17 (1999).
[10] M. N. Iliev, M. V. Abrashev, V. N. Popov, and V. G. Hadjiev, Phys. Rev. B **67**, 212301 (2003).
[11] E. S. Božin, X. Qiu, M. Schmidt, G. Paglia, J. F. Mitchell, P. G. Radaelli, Th. Proffen, and S. J. L. Billinge, Phys. B **385**, 110 (2006).
[12] R. M. Potter and G. R. Rossman, Amer. Miner. **64**, 1199 (1979).
[13] M. N. Iliev, M. V. Abrashev, J. Laverdiere, S. Jandl, M. M. Gospodinov, Y.-Q. Wang, and Y.-Y. Sun, Phys. Rev. B **73**, 064302 (2006).
[14] I. S. Smirnova, A. V. Bazhenov, T. N. Fursova, A. V. Dubovitskii, L. S. Uspenskaya, and M. Yu. Maksimuk, Cond. Mat. Str. El. 2007.
[15] T. Zhang, E. Zhukova, B. Gorshunov, D. Wu, A. S. Prokhorov, V. I. Torgashev, E. G. Maksimov, and M. Dressel, Phys. Rev. B **81**, 125132 (2010).
[16] S. Zouari, M. Ellouze, A. Nasri, W. Cherif, E. K. Hlil, and F. Elhalouani, J. Supercond. Nov. Magn. (2013).
[17] B. Gorshunov, E. Zhukova, V. I. Torgashev, L. S. Kadyrov, L. Motovilova, F. Fischgrabe, V. Moshnyaga, T. Zhang, R. Kremer, U. Pracht, S. Zapf, and M. Dressel, Cond. Matter. Str-El 1303 (2013).
[18] Y. Okimoto, T. Katsufuji, T. Ishikawa, A. Urushibara, T. Amira, and Y. Tokura, Phys. Rev. Lett. **75**, 109 (1995).
[19] K. H. Kim, J. Y. Gu, H. S. Choi, G. W. Park, and T. W. Noh, Phys. Rev. Left. **77**, 1877 (1996).
[20] M. N. Iliev and M. V. Abrashev, J. Raman Spectrosc. **32**, 805 (2001).
[21] V. B. Podobedov, A. Weber, D. B. Romero, J. P. Rice, and H. D. Drew, Solid State Comm. **105**, 589 (1998).
[22] M. N. Iliev, M. V. Abrashev, H. G. Lee, V. N. Popov, Y. Y. Sun, C. Thomsen, R. L. Meng, and C. W. Chu, Phys. Rev. B **57**, 2872 (1998).
[23] M. V. Abrashev, V. G. Ivanov, M. N. Iliev, R. A. Chakalov, R. I. Chakalova, and C. Thomsen, Phys. Stat. Sol. (b) **215**, 631 (1999).
[24] S. Yoon, H. L. Liu, G. Schollerer, S. L. Cooper, P. D. Han, D. A. Payne, S. W. Cheong, and Z. Fisk, Phys. Rev. B **58**, 2795 (1998).
[25] A. Dubroka, J. Humlicek, M. V. Abrashev, Z. V. Popovic, F. Sapina, and A. Cantarero, Phys. Rev. B **73**, 224401 (2006).
[26] N. V. Minh, J. of Phys.: Conference Series **187**, 012011 (2009).
[27] P. Bjornsson, M. Rubhausen, J. Backstrom, M. Kall, S. Eriksson, J. Eriksen, and L. Borjesson, Phys. Rev. B **6**, 1193 (2000).
[28] P. T. Phong, S. J. Jang, B. T. Huy, Y.-I. Lee, and I.-J. Lee, J. Mater. Sci.: Mater Electron **24**, 2292 (2013).
[29] D. Turki, R. Cherif, E. K. Hlil, M. Ellouze, and F. Elhalouani, Int. J. Mod. Phys. B **28**, 1450230 (2014).
[30] F. Moussa, M. Hennion, J. Rodriguez-Carvajal, H. Moudden, L., Pinsard, and A. Revcolevschi, Phys. Rev. B **54**, 15 149 (1996).
[31] M. A. Gilleo, Acta Crystallogr. **10**, 161 (1957).
[32] J. Kanamori, J. Phys. Chem. Solids **10**, 87 (1959).
[33] P. G. Radaelli, G. Iannone, M. Marezio, H. Y. Hwang, S-W. Cheong, J. D. Jorgensen, and D. N. Argyriou, Phys. Rev. B **56**, 13 (1997).
[34] M. Medarde, J. Mesot, P. Lacorre, S. Rosenkranz, P. Fischer, and K. Gobrecht, Phys. Rev. B **52**, 9248 (1995).
[35] V. Ravi, S. D. Kulkarni, V. Samuel, S. N. Kale, J. Mona, R. Rajgopal, A. Daundkar, P. S. Lahoti, and R. S. Joshee, Ceramics Inter. **33**, 1129 (2007).
[36] A. Paolone, P. Roy, A. Pimenov, A. Loidl, O. K. Mel'nikov, and A. Y. Shapiro, Phys. Rev. B **61**, 11255 (2000).
[37] A. Arulraj and C. N. R. Rao, J. Solid State Chem. **145**, 557 (1999).
[38] J. R. Chocha, P. A. Chhelavda, and J. A. Bhalodia, Trans. of The Indian Inst. of Metals **64**, 159 (2011).
[39] M. Kim, H. Barath, S. L. Cooper, P. Abbamonte, E. Fradkin, M. Rübhausen, C. L. Zhang, and S.-W. Cheong, Phys. Rev. B **77**, 134411 (2008).
[40] V. G. Sathe, R. Rawat, A. Dubey, A. V. Narlikar, and D. Prabhakaran, J. Phys.: Condens. Matter **21**, 075603 (2009).
[41] N. V. Minh and I.-S. Yang, Vibrational Spectroscopy **42**, 353 (2006).
[42] S. Zhi-Hui, N. Ting-Yin, Z. Yue-Liang, Z. Song-Qing, and C. Ling-Zhu, Chin. Phys. Lett. **25**, 1861 (2008).
[43] R. Kruger, B. Schulz, S. Naler, R. Rauer, D. Budelmann, J. Backstrom, K. H. Kim, S. W. Cheong, V. Prebeinos, and M. Rubhausen, Phys. Rev. Lett. **92**, 097203-1–097203-4 (2004).
[44] M. Ghiasi and A. Malekzadeh, Sep. and Puri. Tech. **134**, 12 (2014).
[45] C. Gargori, S. Cerro, R. Galindo, A. García, M. Llusar, and G. Monro's, Ceramics Inter. **38**, 4453 (2012).